Non-Orthogonal Multiple Access (NOMA) for Underwater Acoustic Communication

Mohammud J. Bocus, Dimitris Agrafiotis and Angela Doufexi
Department of Electrical and Electronic Engineering, University of Bristol, BS8 1UB, UK.

***Abstract*—In this paper we investigate the application of the non-orthogonal multiple access (NOMA) technique for multiuser underwater acoustic (UWA) communication. The NOMA scheme can be implemented using either orthogonal frequency division multiplexing (OFDM) or filterbank multicarrier (FBMC) modulation for waveform shaping. In order to boost the throughput over a 1 km time-varying underwater acoustic channel (UAC), spatially multiplexed multiple-input multiple-output (MIMO) systems are considered. We evaluate the bit error rate (BER), packet error rate (PER) and maximum bit rate performances of Turbo-coded NOMA-OFDM and NOMA-FBMC systems for a 2-user scenario where both users utilize the same frequency bandwidth. It is shown that while both the NOMA-OFDM and NOMA-FBMC systems show comparable performance in terms of BER and PER, the MIMO NOMA-FBMC system however achieves higher bit rates than the OFDM-based system.**

I. Introduction

Underwater acoustic (UWA) communication has become an active area of research due to developments in oceanography and military applications. In order to meet the demand for future underwater applications where urgent intervention is required, multiple unmanned underwater vehicles can be deployed simultaneously. However, the challenge in a multiuser scenario is to achieve a good trade-off between system throughput and user fairness. As compared to orthogonal multiple access (OMA) schemes such as OFDMA, in non-orthogonal multiple access (NOMA) multiple users use the same time and frequency resources, hence achieving a superior overall spectral efficiency. This makes the NOMA technology very attractive for multiuser UWA communication where the bandwidth is extremely limited.

The basic idea behind NOMA is that the users' signals are superposed in the power domain by exploiting the channel gain difference between them and usually the users with better channel conditions are allocated less power [1]. Then at the receiver end, successive interference cancellation (SIC) is used for multiuser detection and decoding. OFDM or FBMC signaling combined with non-orthogonal user multiplexing can be used to generate the transmit signals for the users. OFDM is very robust against intersymbol interference (ISI) in a multipath channel and it is also a highly bandwidth efficient modulation technique which enables simple frequency domain equalization. The integration of MIMO with OFDM has been found to be an attractive solution for the dynamic and bandwidth-limited UACs since both the data rate and reliability of the system can be enhanced (e.g., [2]). However, the channel impulse response (CIR) can be very long in an UAC and the cyclic prefix (CP) duration should be at least equal to the duration of the CIR. The OFDM symbol duration should also be made very long to maintain a good spectral efficiency. Nevertheless, in fast time-varying UACs, variations across each symbol make the system susceptible to Doppler-induced inter-carrier interference (ICI) [3]. To overcome these disadvantages, cosine modulated multitone (CMT) and filtered multitone (FMT) - based FBMC systems have been recently investigated for single-user UWA communication. For instance, in [4] and [5], it has been shown than FBMC provides a better performance than OFDM in UACs which suffer from both time and frequency dispersions (doubly-dispersive).

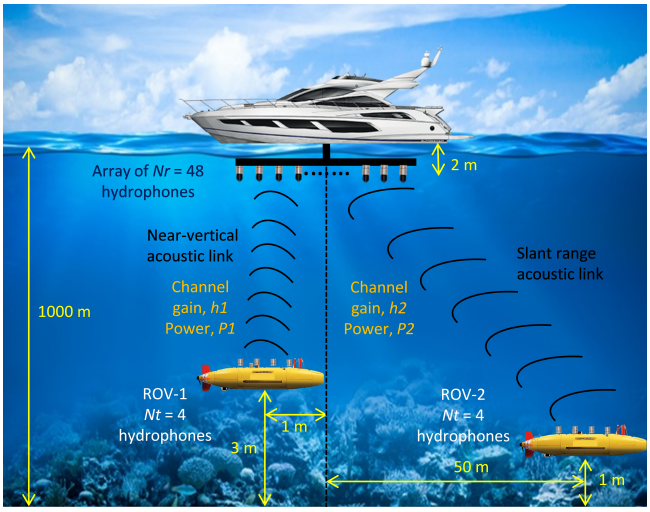

Fig. 1. Target scenario for multiuser UWA communication

The scenario of interest is depicted in Fig. 1 where two remotely operated underwater vehicles (ROVs) communicate simultaneously with a surface vessel over a range of approximately 1 km. Each ROV is equipped with 4 transmitting hydrophones while the surface vessel has an array of 48 receiving hydrophones. The downlink is used for sending control commands to the ROVs while the uplink is used solely for transmitting real-time video to the surface vessel.

In this work, the NOMA technique is investigated for multiuser UWA communication. We examine the BER and PER performance comparison between MIMO NOMA-OFDM and MIMO NOMA-FBMC in a 1 km time-varying UAC. Powerful Turbo codes are also used with the systems to improve the reliability of the communication link. The maximum achievable bit rates with the different systems are also provided. An

FBMC system based on OFDM/offset quadrature amplitude modulation (OFDM/OQAM) is used in this work since the subcarriers maximally overlap and hence 100% bandwidth efficiency is achievable. Moreover, to cope with the imaginary interference in FBMC/OQAM and make its application to MIMO straightforward, a modified FBMC/OQAM system as proposed in [6] is considered. In this system, complex symbols are spread in time to cancel the imaginary interference.

The rest of this paper is organized as follows: The typical properties of an UAC are briefly described in Section II. Section III provides the system model for the modified FBMC/OQAM system and also describes the NOMA concept. The performance evaluation of the systems in terms of BER, PER and maximum achievable bit rate are presented in Section IV. Finally Section V concludes our work.

Notation. $(.)^{\mathsf{T}}$ and $(.)^{\mathsf{H}}$ denote the transpose and Hermitian transpose operations respectively. $\mathbf{I}$ is an identity matrix.

II. Underwater Acoustic Channel

A. Path Loss

The path loss (in dB) for a transmission distance d m and signal frequency f kHz is given by [7]

$$10\log A(d,f) = k.10\log d + d.10\log\alpha(f), \tag{1}$$

where k is the spreading factor which is equal to 1 in shallow water and 2 in deep water and $\alpha(f)$ is the absorption coefficient (in dB/m) which can be calculated for frequencies above a few hundred Hz using the Thorp's formula as follows (as a function of f in kHz) [8]

$$10\log\alpha(f) = (\frac{0.11f^2}{1+f^2}+\frac{44f^2}{4100+f^2}+2.75\times10^{-4}f^2+0.003).10^{-3}. \tag{2}$$

B. Ambient Noise

The major noise sources can be expressed as follows (in dB re μPa per Hz where f is in kHz) [8]

$$\begin{aligned} 10\log N_{tb}(f) &= 17-30\log(f) \\ 10\log N_s(f) &= 40+20(s-0.5)+26\log(f)- \\ &\quad 60\log(f+0.03) \\ 10\log N_w(f) &= 50+7.5w^{0.5}+20\log(f)-40\log(f+0.4) \\ 10\log N_{th}(f) &= -15+20\log(f), \end{aligned} \tag{3}$$

where N_{tb}, N_s, N_w and N_{th} represent turbulence, shipping (s is the shipping factor which takes a value between 0 and 1 for low and high shipping activity respectively), wind (w is the wind speed in m/s) and thermal noise respectively. The total power spectral density (PSD) of ambient noise for a given frequency f (in kHz) is expressed as [7]:

$$N_{all}(f) = N_{tb}(f)+N_s(f)+N_w(f)+N_{th}(f). \tag{4}$$

C. Signal-to-Noise Ratio (SNR)

The SNR can be computed as follows [7]

$$\text{SNR}(d,f) = \frac{S_{tx}(f)}{A(d,f)N_{all}(f)}, \tag{5}$$

where $S_{tx}(f)$ is the transmitted signal PSD whose power can be adjusted to achieve the desired SNR level [9]. Using the factor $1/A(d,f)N_{all}(f)$, an optimum operating frequency can be obtained for each transmitter-receiver separation at which the SNR is maximum.

D. Propagation Delay

The speed of sound (v) in water can be expressed empirically as follows [8]

$$\begin{aligned} v &= 1448.96+4.591\theta-0.05304\theta^2+0.0002374\theta^3 \\ &+ 1.340(S-35)+0.0163z+1.675\times10^{-7}z^2 \\ &- 0.01025\theta(S-35)-7.139\times10^{-13}\theta z^3, \end{aligned} \tag{6}$$

where z is the water depth in m, S is the salinity of water in parts per million (ppm) and θ is the water temperature in ^{o}C. The high propagation delay can cause the delay spread in an UAC (especially horizontally-configured channels) to span over tens or even hundreds of milliseconds [9].

E. Multipath

The CIR for a multipath UAC can be expressed as [7]

$$h(\tau,t) = \sum_r \Omega_r(t)\delta(\tau-\tau_r(t)), \tag{7}$$

where $\Omega_r(t)$ is the time-varying amplitude of the rth path. Assuming the paths' amplitudes are constant within a short data block, we can write $\Omega_r(t)\approx\Omega_r$. Motion at the transmitter and/or receiver results in a Doppler shift which is proportional to the ratio $\xi=v_{txrx}/v$ [9]. ξ denotes the Doppler scale factor and v_{txrx} is the relative velocity between the mobile nodes. Hence, for N_{pa} discrete paths (7) can be re-written as [7]

$$h(\tau,t)=\sum_{r=1}^{N_{pa}}\Omega_r\delta(\tau-[\tau_r-\xi_r t]). \tag{8}$$

III. System Model

A. Low Complexity MIMO-FBMC/OQAM

Conventional FBMC/OQAM systems can achieve a maximum bandwidth efficiency at the expense of intrinsic imaginary interference which makes channel estimation and the application of MIMO challenging. The authors of [6] proposed to spread the symbols in the time (or frequency) domain to cancel the imaginary interference, restore complex orthogonality and ensure a low-complexity implementation since the method is based on Hadamard matrices. Consider an FBMC/OQAM system with L subcarriers and K FBMC symbols. The signal at the transmitter can be expressed as [6]

$$s(t)=\sum_{k=1}^{K}\sum_{l=1}^{L}g_{l,k}(t)x_{l,k}, \tag{9}$$

where $x_{l,k}$ are the symbols transmitted on the lth subcarrier at the kth time slot and $g_{l,k}(t)$ is the time and frequency shifted version of a prototype filter $p(t)$:

$$g_{l,k}(t)=p(t-kT)\mathrm{e}^{\mathrm{j}2\pi lF(t-kT)}\mathrm{e}^{\mathrm{j}\theta_{l,k}}, \tag{10}$$

where $\theta_{l,k}=\frac{\pi}{2}(l+k)$ is the phase shift. The received signal $r(t)$ is then projected on $g_{l,k}(t)$ to obtain the received symbols $y_{l,k}$ as follows [6]

$$y_{l,k}=\langle r(t),g_{l,k}(t)\rangle=\int_{-\infty}^{-\infty} r(t)g^{*}_{l,k}(t)\mathrm{d}t. \tag{11}$$

Although the system is computed from FFT and a polyphase network, the expression in (9) is represented in matrix notation (for ease of analytical understanding) as follows

$$\mathbf{s}=\mathbf{G}\mathbf{x}. \tag{12}$$

where the column vectors of $\mathbf{G}$ represent the sampled pulses $g_{l,k}(t)$ and $\mathbf{x}$ is the transmitted symbol vector defined as

$$\mathbf{x}=\begin{bmatrix}x_{1,1} & x_{2,1}\cdots x_{L,1} & x_{1,2}\cdots x_{L,K}\end{bmatrix}^{\mathrm{T}}. \tag{13}$$

The received signal vector can be expressed as

$$\begin{aligned}\mathbf{y}&=\mathbf{D}\mathbf{x}+\mathbf{n}\\&=\begin{bmatrix}y_{1,1} & y_{2,1}\cdots y_{L,1} & y_{1,2}\cdots y_{L,K}\end{bmatrix}^{\mathrm{T}},\end{aligned} \tag{14}$$

where $\mathbf{n}$ is the noise vector and $\mathbf{D}$ is the transmission matrix which is computed as

$$\mathbf{D}=\mathbf{G}^{\mathsf{H}}\mathbf{G}. \tag{15}$$

In FBMC, $\mathbf{D}$ is not an identity matrix due to the imaginary interference observed at the off-diagonal elements [6]. An identity matrix can be obtained by taking only the real part of $\mathbf{D}$. Thus, only $\frac{LK}{2}$ complex symbols can be transmitted. For the spreading process, the uncorrelated data symbols $\tilde{\mathbf{x}}$ are precoded using a unitary coding matrix $\mathbf{C}$ such that the transmitted symbols are computed as [6]

$$\mathbf{x}=\mathbf{C}\tilde{\mathbf{x}}. \tag{16}$$

The imaginary interference is canceled by choosing the coding matrix to satisfy the following condition [6]

$$\mathbf{C}^{\mathsf{H}}\mathbf{D}\mathbf{C}=\mathbf{I}, \tag{17}$$

At the receiver, decoding is performed on the received data symbols as follows

$$\tilde{\mathbf{y}}=\mathbf{C}^{\mathsf{H}}\mathbf{y}. \tag{18}$$

The coding matrix $\mathbf{C}$ can be generated by choosing $\frac{K}{2}$ suitable column vectors from a Hadamard matrix of order K which are then used to spread the symbols in the time domain. This is done for all subcarriers until a coding matrix of size $LK\times\frac{LK}{2}$ which satisfies (17) is obtained.

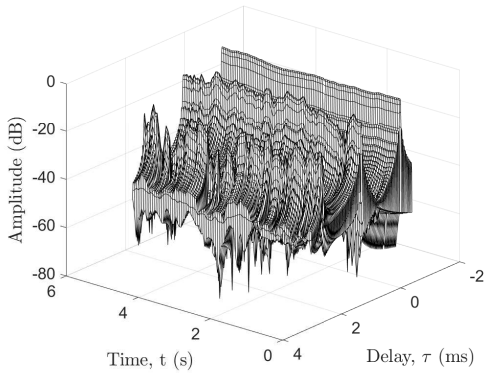

(a)

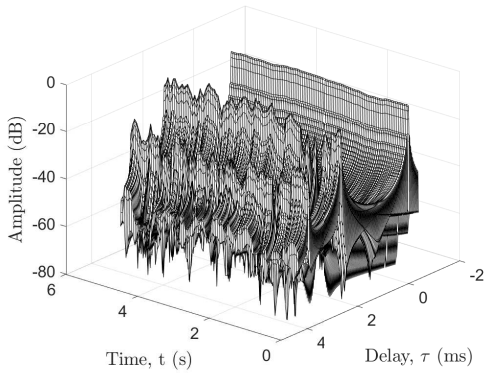

(b)

Fig. 2. A typical channel response between BS and (a) ROV 1 (b) ROV 2

B. NOMA

In NOMA, all the subcarriers in the system are assigned to each user. Hence the bandwidth resources which are assigned to the user in poor channel conditions are also available to the user in strong channel conditions, significantly improving the spectral efficiency [10]. In our scenario, each ROV utilizes the same spectrum resources to transmit simultaneously in the uplink to a base-station (BS) which is located at the surface.

Consider a single-input single-output system (SISO) where the signal transmitted by ROV-i (i=1, 2) is denoted as x_i, where E[$|x_i|^2$]=1, and the transmit power is P_i. The superposed received signal at the BS can be expressed as

$$y=h_1\sqrt{P_1}x_1+h_2\sqrt{P_2}x_2+n, \tag{19}$$

where h_i is the complex channel coefficient between ROV-i and the BS and n represents the noise and interference observed at the BS with a PSD of N_0. In Fig. 1, ROV 1 experiences a higher channel gain than ROV 2, hence $|h_1|^2/N_0>|h_2|^2/N_0$.

NOMA can be combined with MIMO to further improve the system performance. Consider an uplink MIMO system with N_r receive hydrophones at the BS and N_t transmitting hydrophones at each ROV. In the uplink, the signal from the user with the higher channel gain (strong user) is decoded

TABLE I
SIMULATION PARAMETERS

Parameters	ROV 1	ROV 2
Bandwidth	25 kHz	
Carrier frequency	32.5 kHz	
Water depth	1000 m	
TX height from sea-floor	3 m	1 m
RX height from sea-floor	998 m	
Number of TX, N_t	4	
Number of RX, N_r	48	
Subcarriers	256	
Delay spread	2.6 ms	3.9 ms
OFDM CP duration	5.12 ms	
Modulation	16-QAM	
Turbo code rate	1/3	
Relative velocity	≈1.5 m/s	
Doppler frequency	≈32.5 Hz	
Average channel gain	≈-27 dB	≈-32 dB
NOMA power allocation factor	0.4	0.6

with interference first. Then, the signal from the user with the weaker channel gain (weak user) is decoded free from interference [11]. Thus, the received signal vectors for the two ROVs at the BS can be expressed as

$$\mathbf{y}_1=\mathbf{H}_1\sqrt{P_2}\mathbf{x}_1+\mathbf{H}_2\sqrt{P_2}\mathbf{x}_2+\mathbf{n}, \tag{20}$$

$$\mathbf{y}_2=\mathbf{y}_1-(\mathbf{H}_1\sqrt{P_1}\hat{\mathbf{x}}_1)+\mathbf{n}, \tag{21}$$

where $\mathbf{y}_i$ is the $N_r\times 1$ received signal vector for ROV-i, $\mathbf{x}_i$ is the $N_t\times 1$ transmitted symbol vector for ROV-i, $\mathbf{H}_i$ is the $N_r\times N_t$ channel matrix for ROV-i, $\mathbf{n}$ is the $N_r\times 1$ noise vector and P_i is the power allocation factor for ROV-i. At the receiver side, a zero-forcing (ZF) or minimum mean squared error (MMSE) detection matrix can be used to decode the signals, $\hat{\mathbf{x}}_i$. The detection matrix can be generated by the BS using the channel state information (CSI) from the two ROVs. Assuming MMSE, the detection matrix of the channel matrices $\mathbf{H}_1$ and $\mathbf{H}_2$ is given by

$$\mathbf{W}_i=\left(\mathbf{H}_i\mathbf{H}_i^H+\rho^{-1}\mathbf{I}_{N_t}\right)^{-1}, \tag{22}$$

where $\mathbf{I}_{N_t}$ is an $N_t\times N_t$ identity matrix and ρ is the receive SNR at the BS. The detected symbol vectors for ROV-i is thus given by

$$\hat{\mathbf{x}}_i=\mathbf{W}_i\mathbf{y}_i. \tag{23}$$

IV. SIMULATION RESULTS

The simulation parameters are summarized in Table 1 while the physical setup of the transmission scenario is illustrated in Fig. 1. The channel coefficients are generated using a statistical UAC model as in [12] where the Doppler spread is assumed to increase linearly from 0.5 Hz to 2 Hz with the channel taps. Typical channel responses as observed by the two ROVs are illustrated in Fig. 2.

The BER and PER performances for the two ROVs using Turbo-coded 4×48 NOMA-OFDM and NOMA-FBMC/OQAM signaling are shown in Fig. 3 and 4 respectively. For comparison purposes only, the BER performances

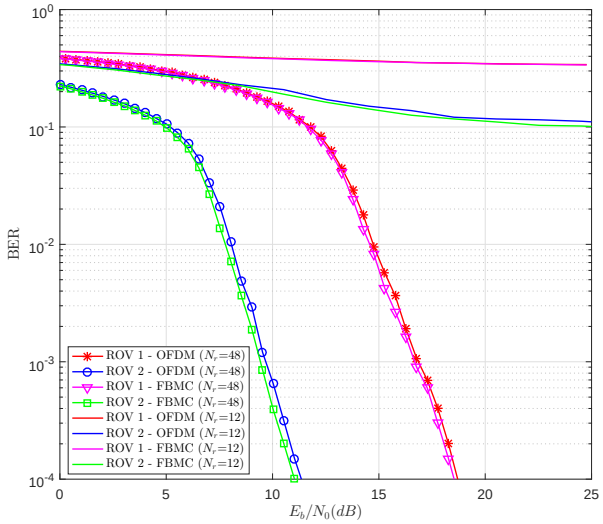

Fig. 3. BER performance of Turbo-coded NOMA-FBMC/OQAM and NOMA-OFDM systems in the UAC

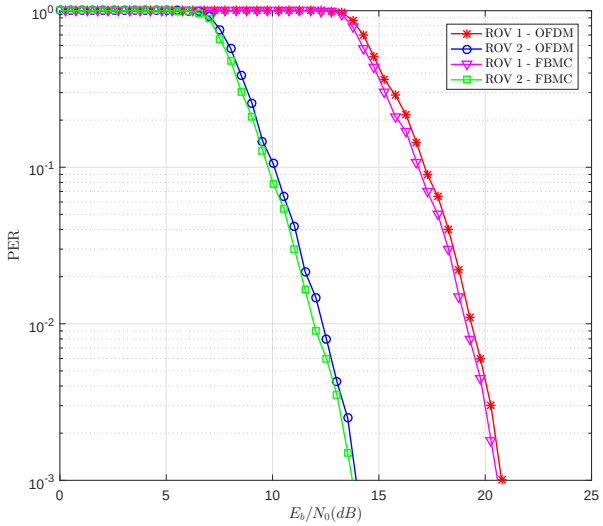

Fig. 4. PER performance of Turbo-coded NOMA-FBMC/OQAM and NOMA-OFDM systems in the UAC

of 4×12 NOMA systems in the same channel and using the same parameters as the 4×48 systems are included in Fig. 3. This type of MIMO configuration is often used for single-user UWA communication (e.g., [2]). In order to better represent the real-world UAC, colored noise is used in the simulations instead of additive white Gaussian noise (AWGN). Packet-based transmission is considered for both the FBMC/OQAM and OFDM systems. For the FBMC/OQAM system, a Hermite-based prototype filter with an overlapping factor of 4 is considered. Also, the time spreading can cause interference between packets and hence a guard (zero) time-

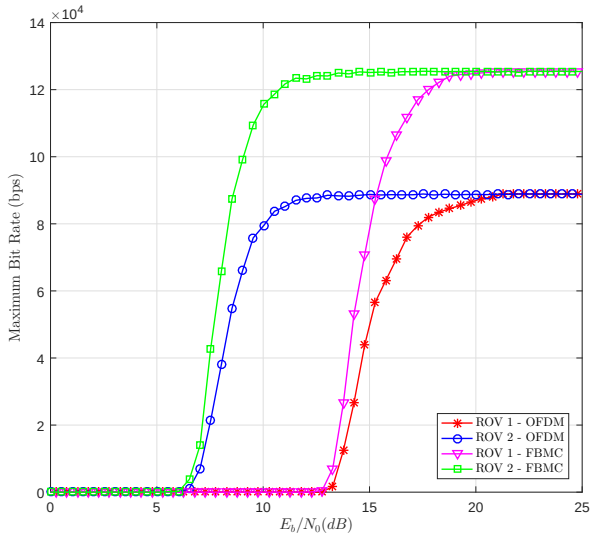

Fig. 5. Maximum achievable bit rates for the two ROVs in the UAC

slot is included between each packet. A spreading factor of 16 FBMC (real) symbols is used so that we have 8 symbols per subcarrier as described in Section III.

It can be observed from Fig. 3 that for both ROVs, the 4×12 NOMA systems achieve a high error rate. This justifies the use of a larger receiving array (N_r=48) for our scenario. Furthermore, the SINR for each user can be improved when the number of receiving hydrophones is increased [3]. In Fig. 3 and Fig. 4, the FBMC system achieves a marginal improvement over the OFDM system. However, this shows that FBMC system can achieve robust performance in a time-varying frequency-selective channel without using any CP. Also, the absence of a CP implies that more useful bits can be transmitted per second compared to OFDM. Considering the 4×48 NOMA-FBMC system in Fig. 3, ROV-2 achieves around 7.5 dB better performance than ROV-1 at a BER of 10^{-4}. It can be inferred that although ROV-2 suffers from weaker channel conditions, the BS can successfully decode its message signal using SIC as the interference from ROV-1 can be overcome using a greater power allocation for ROV-2.

According to the PER, the maximum achievable bit rate for the two ROVs can be calculated as follows [13]

$$\text{bit rate} = \frac{(1-\text{PER})\times\eta_{bit/packet}}{T_{packet}(s)}, \tag{24}$$

where $\eta_{bit/packet}$ is the number of bits per packet and T_{packet} is the packet duration. Considering the simulation parameters in Table I and the PER performance in Fig. 4, the maximum throughput that can be achieved for the two ROVs using OFDM and FBMC/OQAM signaling in our scenario is shown in Fig. 5. It is to be noted that the guard time-slots which are inserted in the FBMC/OQAM system cause a bandwidth efficiency loss of $\frac{1}{K+1}$ [6]. Despite this loss, we observe from Fig. 5 that for both ROVs, the improvement in bit rate with NOMA-FBMC/OQAM (125.5 kbps) compared to NOMA-OFDM (88.72 kbps) is approximately 41.5%.

V. Conclusion

FBMC/OQAM can achieve robust performance in a doubly-dispersive UAC without using a CP, owing to the good time and frequency localization property of its prototype filter. In this work we have noted a significant increase in bit rate with FBMC/OQAM compared to OFDM for similar simulation parameters. This makes real-time video transmission over the 1 km UAC with acceptable video quality a potentiality. By deploying several ROVs simultaneously, more data can be captured and transmitted to the surface within a shorter period of time. This can be very useful for applications where immediate action needs to be taken, for example, repairing an oil leak on a pipe under an offshore oil rig. By exploiting the power domain in NOMA, a good trade-off between user fairness and system throughput is achieved for all users which are located in both good and poor channel conditions.

References

[1] S. Ali, E. Hossain, and D. I. Kim, "Non-orthogonal multiple access (NOMA) for downlink multiuser MIMO systems: User clustering, beamforming, and power allocation," *IEEE Access*, vol. 5, pp. 565–577, 2017.

[2] B. Li *et al.*, "MIMO-OFDM for high-rate underwater acoustic communications," *IEEE Journal of Oceanic Engineering*, vol. 34, no. 4, pp. 634–644, Oct. 2009.

[3] A. Aminjavaheri and B. Farhang-Boroujeny, "UWA massive MIMO communications," in *OCEANS 2015 - MTS/IEEE Washington*, Oct 2015, pp. 1–6.

[4] P. Amini *et al.*, "Filterbank multicarrier communications for underwater acoustic channels," *Oceanic Engineering, IEEE Journal of*, vol. 40, no. 1, pp. 115–130, 2015.

[5] J. Gomes and M. Stojanovic, "Performance analysis of filtered multitone modulation systems for underwater communication," in *OCEANS 2009, MTS/IEEE Biloxi-Marine Technology for Our Future: Global and Local Challenges*. IEEE, 2009, pp. 1–9.

[6] R. Nissel and M. Rupp, "Enabling low-complexity MIMO in FBMC-OQAM," in *2016 IEEE Globecom Workshops (GC Wkshps)*, Dec 2016, pp. 1–6.

[7] H. Esmaiel and D. Jiang, "Review article: Multicarrier communication for underwater acoustic channel," *Int'l J. of Communications, Network and System Sciences*, vol. 6, no. 08, p. 361, 2013.

[8] M. C. Domingo, "Overview of channel models for underwater wireless communication networks," *Physical Communication*, vol. 1, no. 3, pp. 163–182, 2008.

[9] M. Stojanovic and J. Preisig, "Underwater acoustic communication channels: Propagation models and statistical characterization," *IEEE Communications Magazine*, vol. 47, no. 1, pp. 84–89, Jan. 2009.

[10] Z. Ding, Y. Liu, J. Choi, Q. Sun, M. Elkashlan, I. Chih-Lin, and H. V. Poor, "Application of non-orthogonal multiple access in lte and 5g networks," *IEEE Communications Magazine*, vol. 55, no. 2, pp. 185–191, 2017.

[11] S. Qureshi and S. A. Hassan, "MIMO uplink NOMA with successive bandwidth division," in *Proc. IEEE Wireless Communications and Networking Conf*, Apr. 2016, pp. 1–6.

[12] F. X. Socheleau *et al.*, "A maximum entropy framework for statistical modeling of underwater acoustic communication channels," in *Proc. OCEANS 2010 IEEE - Sydney*, May 2010, pp. 1–7.

[13] X. Su, H. Yu, W. Kim, C. Choi, and D. Choi, "Interference cancellation for non-orthogonal multiple access used in future wireless mobile networks," *EURASIP Journal on Wireless Communications and Networking*, vol. 2016, no. 1, p. 231, 2016.